ORIGINAL RESEARCH PAPER

Science

Volume - 7 | Issue - 1 | January - 2017 | ISSN - 2249-555X | IF : 3.919 | IC Value : 79.96

Push-pull structures of symmetric silane derivatives as a novel hosting materials

KEYWORDS

silane derivatives, luminescent materials, organic light-emitting diode, Stille coupling, Suzuki condensation, molecular modeling, EPR, electrochemistry

Dorota Zajac

Wrocław University of Science and Technology, Faculty of Chemistry, Wybrzeże Wyspiańskiego 27, 50-370 Wrocław, Poland.

Jadwiga Soloducho

Wrocław University of Science and Technology, Faculty of Chemistry, Wybrzeże Wyspiańskiego 27, 50-370 Wrocław, Poland

Tomasz Jarosz

Centre of Polymer and Carbon Materials of the Polish Academy of Sciences, M. Curie-Sklodowskiej 34, 41-819 Zabrze, Poland.

Mieczysław Łapkowski

Silesian University of Science and Technology, Faculty of Chemistry, Strzody 9, 44-100 Gliwice, Poland

Szczepan Roszak

Wrocław University of Science and Technology, Faculty of Chemistry, Wybrzeże Wyspiańskiego 27, 50-370 Wrocław, Poland.

ABSTRACT *Silane-based symmetric* **(4a-g, 9a-c)** *conjugated systems including electron rich heterocycle rings were designed and efficiently synthesized by the Suzuki/Stille condensation and Ullmann reaction. The structures characterize with a comparatively small band gaps and indicate deep absorption in the region 230-500 nm. Moreover, synthesized derivatives reveal light emission in practically the whole visible light. The electrochemical survey disclosed the onset of the oxidation signal was found at relatively low potentials. The band gap (1.55 eV – 2.64 eV) creates the structures potentially suitable as a hosting medium for emitters. The lowest electrochemical and optical band gap describes dithienosiloles, the largest - structure with tetraphenylsilane group. The electrochemical character of dithienosilole/tetraphenylsilane blocks was also certified by EPR as well as theoretical studies. The calculations explain the contrast between electrochemical and optical experimentally estimated energy gaps.*

1. Introduction

Fluorescent organic conjugated molecules based on dithienosilole fragments due to their unique optical and electronic properties, have been the subject of active research in advanced materials such as organic light-emitting diodes (OLEDs) [1-4], chemical sensors [5-9], photovoltaic devices [10-14], organic thin-film transistors (OTFTs) [15,16]. Actually, dithienosiloles attract much attention due to their high photoluminescence quantum efficiency in both, solution and the solid state.

Siloles possess a low-lying LUMO level, compared to other cyclopentadiene analogues, due to the interaction between the σ* orbital of the silylene fragment, effectively interacting with the π* orbital of the butadiene fragment [17]. Furthermore, the silicon atom stabilizes the highest occupied molecular orbital (HOMO) compared to the carbon counterparts [18], thus siloles exhibit high thermodynamical stability in the air [10]. Additionally, the longer Si-C bond (~0.3 Å) modifies the geometry of the fused dithophene unit [19] results in highly efficient electron-transporting properties in organic light-emitting diodes (OLEDs), compared to the standard electron transport material Alq_3 (q=8-hydroxyquinolinato) [20].

The development of novel materials with competitive electroluminescent parameters requires the searching for new D–A systems with optimized properties. To address this need, we have designed and synthesized new small molecules **4a-g** based on an electron-reach dithienosilole (Scheme 1), flanked by arylene fragments, such as benzofurazan, thiophene, furan, thiazole, phenyl and pyridine. In this work we report also the electrochemical and spectroscopic properties of synthesized macromolecular structures.

2. Methodological Part

2.1. Materials and Instruments

n-Butyllithium (2.5M in hexane), 1,4-dibromobenzene (99%), copper(I) iodide (99.9%), 1,10-phenanthroline (99%), 9(10H)-acridanone (99%), 4-methoxyphenylboronic acid (95.0%), 2-isopropoxy-4,4,5,5-tetramethyl-2,1,3-dioxoborolane (98%), tetrakis (triphenylphosphine)- palladium(0) (99%), 5-hexylthiophene-2-boronic acid pinacol ester (95%), 2-(tributylstannyl) thiazole (97%), 2- (tributylstannyl)furan (97%), 2- (tributylstannyl)thiophene (97%) were received from Aldrich. Phenyltributylstannane (97%) was purchased from Fluka, 2-tri-n-butylstannylpyridine (80%) was received from Alfa Aesar. 5-(4,4,5,5-Tetramethyl-1,3,2-dioxaborolan-2-yl)benzofurazan (97%) was purchased from Acros Organics. Anhydrous potassium carbonate (99%) was received from Chempur. Anhydrous tetrahydrofuran was purchased from POCH. Tetrahydrofuran was dried over sodium/benzophenone ketal prior to be used. Other commercially available reagents were used without the earlier purification. Preparative column chromatography was accomplished on the glass column with Fluka silica gel for flash chromatography, 220-440 mesh. 600 MHz ^{1}H NMR and ^{13}C NMR spectra were registered in deuterated chloroform ($CDCl_3$) on Bruker Avance II 600 Instruments. Chemical shifts were locked to chloroform δ_H 7.26 (s) and δ_C 77.16 (t) signals.

Electrochemical investigations were estimated in 0.1 M solutions of Bu_4NBF_4 in dichloromethane (CH_2Cl_2, DCM) solvent, at room temperature. The electrochemical study was carried out using the potentiostat Autolab PGSTAT20 (Metrohm Autolab). The electrochemical cell equipped with the platinum disk with 1 mm diameter of a working area as a working electrode and ITO glass as a working electrode, a Ag/AgCl electrode as a reference electrode and a platinum coil as an auxiliary electrode. Cyclic voltammetry measurements were handled at room temperature under argon with

Volume - 7 | Issue - 1 | January - 2017 | ISSN - 2249-555X | IF : 3.919 | IC Value : 79.96

a 50 mV/s and 300 mV/s scan rate, in oxidation and reduction range. Potentials were calibrated vs ferrocene/ferrocenium redox couple. Fluorescence measurements were recorded on the Hitachi F-2500 fluorescence spectrometer. Samples for electrochemical and spectroelectrochemical studies were dissolved in 0.1M tetrabutylammonium tetrafluoroborate (Sigma-Aldrich, >99.0%, electrochemical analysis grade) in dichloromethane (Sigma-Aldrich, CHROMASOLV, >99.9%, HPLC grade), working as a supporting electrolyte. Each of the structures was regarded individually (c=1mM). Electrochemical measurements of 4a-g were estimated using a standard three-electrode cell, with a Pt or indium-tin oxide (ITO) working electrode, an Ag pseudo-reference electrode and a Pt coil counter electrode. Investigations were carried out on a Metrohm-Autolab PGSTAT100N potentiostat. Before the measurement, every sample was purged with inert gas, while the same gas was being passed over the experimental solution during the study. UV-Vis-NIR spectroelectrochemical investigations were estimated in a 2mm Hellma QS cuvette, using ITO coated quartz slides (Precision Glass & Optics, 20+/-5 Ω/sq, 9 × 60 × 1 mm) as the working electrode, an Ag pseudo-reference electrode and a Pt mesh counter electrode. UV-Vis-NIR spectra were recorded using an Ocean Optics diode-array spectrometers set (QE65000 and NIRQuest 512). Electron Paramagnetic Resonance (EPR) spectra were registered using a JEOL JES FA-200 X band spectrometer. A capillary spectroelectrochemical cell was utilized also, with the same electrode configuration as in the standard electrochemical investigations. Potentials applied in all of the measurements were calibrated vs the ferrocene/ferrocinium redox couple and, unless stated otherwise, are shown in relation to this reference. The dilute solutions of synthesized compounds in dichloromethane were prepared at a concentration 10^{-6} mol/dm^3. Absorption spectra were recorded with Spectroquant Pharo 300 spectrometer. Fluorescence investigations were performed on the Hitachi F-4500 fluorescence spectrometer.

2.2. Synthesis

2.2.1. 4-Octyl-4-methyl-dithienosilole (2)

3,3'-Dibromo-5,5'-bis(trimethylsilyl)-2,2'-bithiophene (1) (5.00 g, 10.67 mmol) was dissolved in dry THF (100 mL) and cooled to -78°C. To the solution was dropwise added n-BuLi (9.00 ml, 22.41 mmol, 2.5M in hexane). After stirring for 30 min, octylmethyldichlorosilane (3.00 mL, 12.81 mmol) was added dropwise in one portion and stirred for 30 min. Then the reaction mixture was warmed to room temperature and stirred overnight. The mixture was then poured into water and extracted several times with ethyl acetate. The volatiles were evaporated in vacuum. The crude product was purified chromatographically (SiO_2: hexane) to give a green oil (3.37 g, 98%).

^{1}H NMR (600 MHz, CDCl3), δ (ppm): δ 7.26 – 7.25 (d, J = 6.0 Hz, 2H), 7.14 – 7.13 (d, J = 6.0 Hz, 2H), 1.53 – 1.48 (m, 2H), 1.39 – 1.31 (m, 12H), 0.97 – 0.95 (t, J = 6.0 Hz, 3H), 0.47 (s, 3H).

2.2.2. 4-Octyl-4-methyl-5,5'-dibromodithienosilole (3)

NBS (4.10 g, 23.02 mmol) was added in one portion to a solution of 2 (3.04 g, 10.46 mmol) in $CHCl_3$ (140 mL). After being stirred at ambient temperature for 20 h, the mixture was extracted with ethyl acetate. Solvent was evaporated in vacuum and purified with column chromatography (SiO_2: hexane) to obtain 3.50 g of green oil with 70 % yield.

^{1}H NMR (600 MHz, $CDCl_3$), δ (ppm): δ 7.04 (s, 2H), 1.42 – 1.39 (m, 2H), 1.32 – 1.26 (m, 12H), 0.92 – 0.90 (t, J = 6.0 Hz, 3H), 0.40 (s, 3H).

2.2.3. 2,6-Bis(5-benzofurazano)-4-methyl-4-octyl-dithienosilole (4a)

To a mixture of 3 (1.00 g, 2.23 mmol), potasium carbonate (0.925 g, 6.69 mmol), and 5-(4,4,5,5-tetramethyl-1,3,2-dioxaborolan-2-yl)benzofurazan (a) (1.21 g, 4.91 mmol) in toluene (40 mL), MeOH (8 mL), and water (8 mL) was added tetrakis (triphenylphosphine) palladium ($Pd(PPh_3)_4$) (0.129 g, 0.112 mmol) at room temperature. The resulting mixture was refluxed with stirring overnight under nitrogen atmosphere. Then the reaction mixture was concentrated under reduced pressure, diluted with water, and extracted with EtOAc. The extract was washed with brine, dried over $MgSO_4$, and concentrated. The residue was purified by silica gel column chromatography (hexane-EtOAc) to give 4a (0.60 g, 54%) as a red solid.

^{1}H NMR (600 MHz, $CDCl_3$), δ (ppm): δ 7.95 (s, 2H), 7.89 – 7.88 (d, J = 6.0 Hz, 2H), 7.79 – 7.77 (d, J = 12.0 Hz, 2H), 7.56 (s, 2H), 1.30 – 1.26 (m, 12H), 1.05 – 1.02 (t, J = 9.0 Hz, 2H), 0.88 – 0.86 (t, J = 6.0 Hz, 3H), 0.54 (s, 3H).

^{13}C NMR (151 MHz, $CDCl_3$), δ (ppm): δ 150.08, 149.63, 149.33, 148.47, 145.28, 143.63, 142.55, 136.95, 135.73, 135.18, 132.77, 132.20, 131.36, 131.34, 128.74, 124.92, 117.56, 116.85, 110.95, 109.13, 33.33, 33.13, 31.86, 29.24, 29.19, 24.16, 22.67, 14.12, 13.10.

2.2.4. 2,6-Bis(5-hexyltiophen-2-yl)-4-methyl-4-octyl-dithienosilole (4b)

This compound was prepared by using the same procedure as for 2,6-bis(5-benzofurazano)-4-methyl-4-octyl-dithienosilole (4a); (1.21 g, 2.53 mmol) of 3, potasium carbonate (1.05 g, 7.59 mmol), 5-hexylthiophene -2-boronic acid pinacol ester (b) (1.64 g, 5.58 mmol) and tetrakis(triphenylphosphine)palladium (Pd(PPh3)4) (0.146 g, 0.126 mmol). The residue was purified by silica gel column chromatography (hexane-EtOAc) to give 4b (0.58 g, 35%) as a dark orange oil.

^{1}H NMR (600 MHz, CDCl3), δ (ppm): δ 7.08 (s, 2H), 6.98 (d, 2H), 6.70 (d, J = 3.0 Hz, 2H), 2.83 – 2.81 (t, J = 6.0Hz, 4H), 1.72 – 1.68 (m, 4H), 1.36 – 1.27 (m, 24H), 0.94 – 0.88 (m, 11H), 0.43 (s, 3H).

^{13}C NMR (151 MHz, CDCl3), δ (ppm): δ 147.18, 145.01, 144.67, 143.47, 143.08, 138.70, 135.37, 135.04, 129.50, 128.81, 126.97, 125.48, 124.82, 124.59, 122.93, 122.60, 33.53, 33.17, 31.94, 31.65, 31.63, 30.25, 31.21, 29.78, 29.31, 29.26, 24.18, 22.74, 22.65, 14.15, 13.30.

2.2.5. *2,6-Bis(pyridin-2-yl)-4-methyl-4-octyl-dithienosilole (4c)*

To a mixture of 3 (1.66 g, 3.48 mmol) and 2-(tributylstannyl)pyridine (c) (3.34 ml, 10.43 mmol) in anhydrous THF (50 mL) was added tetrakis(triphenylphosphine)palladium ($Pd(PPh_3)_4$) (0.804 g, 0.696 mmol) at room temperature under nitrogen atmosphere. The resulting mixture was refluxed with stirring for 72 h. Then the reaction mixture was concentrated under reduced pressure, diluted with water, and extracted with EtOAc. The extract was washed with brine, dried over $MgSO_4$, and concentrated. The residue was purified by silica gel column chromatography (hexane-EtOAc) to give 4c (0.55 g, 33%) as a brown oil.

^{1}H NMR (600 MHz, CDCl3), δ (ppm): δ 7.60 – 7.57 (m, 4H), 7.37 – 7.35 (t, J = 6.0 Hz, 2H), 7.28 (s, 2H), 7.27 (s, 2H), 1.31 – 1.27 (m, 12H), 0.97 – 0.94 (t, J = 7.5 Hz, 2H), 0.93 – 0.91 (t, J = 6.0 Hz, 3H), 0.12 (s, 3H).

^{13}C NMR (151 MHz, CDCl3), δ (ppm): δ 152.14, 151.72, 146.54, 141.95, 137.59, 135.20, 134.71, 132.10, 131.74, 131.56, 131.22, 130.91, 130.42, 130.08, 128.60, 128.52, 127.94, 107.49, 33.43, 31.95, 29.31, 28.22, 24.25, 22.71, 14.20, 13.66, 13.44.

2.2.6. 2,6-Bis(thiazol-2-yl)-4-methyl-4-octyl-dithienosilole (4d)

This compound was prepared by using the same procedure as for 2,6-bis(pyridin-2-yl)-4-methyl-4-octyl-dithienosilole (4c); (1.00 g, 2.09 mmol) of 3, 2-(tributylstannyl)thiazole (d) (2.00 ml, 6.27 mmol) and tetrakis(triphenylphosphine)palladium ($Pd(PPh_3)_4$) (0.483 g, 0.418 mmol). The resulting mixture was refluxed with stirring for 72 h. The residue was purified by silica gel column chromatography (hexane-EtOAc) to give 4d (0.38 g, 37%) as a yellow-green oil.

^{1}H NMR (600 MHz, CDCl3), δ (ppm): δ 7.79 (d, J = 3.0 Hz, 2H), 7.54 (s, 2H), 7.27 (d, J = 3.0 Hz, 2H), 1.30 – 1.26 (m, 12H), 0.96 – 0.94 (t, J = 6.0 Hz, 2H), 0.89 – 0.87 (t, J = 6.0 Hz, 3H),0.49 (s, 3H).

^{13}C NMR (151 MHz, CDCl3), δ (ppm): δ 161.83, 150.32, 144.49, 143.36, 138.85, 132.28, 132.15, 132.08, 132.03, 129.43, 129.11, 128.57, 128.49,

Volume - 7 | Issue - 1 | January - 2017 | ISSN - 2249-555X | IF : 3.919 | IC Value : 79.96

117.79, 33.10, 31.86, 27.07, 26.86, 26.65, 24.07, 22.66, 17.55, 13.62.

2.2.7. 2,6-Bis(furan-2-yl)-4-methyl-4-octyl-dithienosilole (4e)
This compound was prepared by using the same procedure as for 2,6-bis(pyridin-2-yl)-4-methyl-4-octyl-dithienosilole (4c); (1.00 g, 2.09 mmol) of 3, 2-(tributylstannyl)furan (e) (2.00 ml, 6.27 mmol) and tetrakis(triphenylphosphine)palladium (Pd(PPh3)4) (0.483 g, 0.418 mmol). The resulting mixture was refluxed with stirring for 72 h. The residue was purified by silica gel column chromatography (hexane-EtOAc) to give 4e (0.35 g, 37%) as a dark green oil.

^{1}H NMR (600 MHz, CDCl3), δ (ppm): δ 7.43 (s, 2H), 7.25 (s, 2H), 6.50 – 6.48 (d, J = 12.0 Hz, 4H), 1.32 – 1.26 (m, 12H), 0.96 – 0.94 (t, J = 6.0 Hz, 2H), 0.90 – 0.88 (t, J = 6.0 Hz, 3H), 0.45 (s, 3H).

^{13}C NMR (151 MHz, CDCl3), δ (ppm): δ 149.46, 147.58, 143.32, 142.02, 141.87, 141.54, 141.03, 134.39, 125.07, 120.55, 111.80, 111.50, 107.50, 105.74, 105.51, 104.86, 33.11, 31.93, 29.22, 29.19, 24.10, 22.66, 14.10, 13.83, 13.21.

2.2.8. 2,6-Bis(thiophen-2-yl)-4-methyl-4-octyl-dithienosilole (4f)
This compound was prepared by using the same procedure as for 2,6-bis(pyridin-2-yl)-4-methyl-4-octyl-dithienosilole (4c); (1.00 g, 2.09 mmol) of 3, 2-(tributylstannyl)thiophene (f) (2.00 ml, 6.27 mmol) and tetrakis(triphenylphosphine)palladium (Pd(PPh3)4) (0.483 g, 0.418 mmol). The resulting mixture was refluxed with stirring for 72 h. The residue was purified by silica gel column chromatography (hexane-EtOAc) to give 4f (0.34 g, 34%) as a dark red oil.

^{1}H NMR (600 MHz, $CDCl_3$), δ (ppm): δ δ 7.23 – 7.22 (d, J = 6.0 Hz, 2H), 7.19 – 7.18 (t, J = 6.0 Hz, 4H), 7.06 – 7.04 (t, J = 6.0 Hz, 2H), 1.31 – 1.27 (m, 12H), 0.97 – 0.95 (t, J = 6.0 Hz, 2H), 0.91 – 0.88 (t, J = 9.0 Hz, 3H), 0.46 (s, 3H).

^{13}C NMR (151 MHz, $CDCl_3$), δ (ppm): δ 147.60, 144.81, 143.38, 138.21, 137.60, 129.37, 127.92, 127.86, 126.27, 125.43, 124.43, 124.01, 123.90, 123.32, 123.24, 123.05, 33.12, 31.88, 29.24, 29.20, 24.12, 22.68, 14.11, 13.27, 13.23.

2.2.9. 2,6-Bis(phenyl)-4-methyl-4-octyl-dithienosilole (4g)
This compound was prepared by using the same procedure as for 2,6-bis(pyridin-2-yl)-4-methyl-4-octyl-dithienosilole (4c); (1.00 g, 2.09 mmol) of 3, 2-(tributylstannyl)phenyl (g) (2.05 ml, 6.27 mmol) and tetrakis(triphenylphosphine)palladium (Pd(PPh3)4) (0.483 g, 0.418 mmol). The resulting mixture was refluxed with stirring for 72 h. The residue was purified by silica gel column chromatography (hexane-EtOAc) to give 4g (0.411g, 42%) as a brown solid. Mp = 162-164°C.

^{1}H NMR (600 MHz, $CDCl_3$), δ (ppm): δ 7.60 – 7.57 (m, 4H), 7.36 – 7.35 (d, J = 6.0 Hz, 4H), 7.30 (s, 2H), 7.27 (s, 2H), 1.31 – 1.27 (m, 12H), 0.97 – 0.94 (t, J = 9.0 Hz, 2H), 0.93 – 0.91 (t, J = 6.0 Hz, 3H), 0.12 (s, 3H).

^{13}C NMR (151 MHz, $CDCl_3$), δ (ppm): 152.08, 151.68, 141.94, 141.91, 137.54, 135.17, 134.63, 134.59, 131.53, 131.19, 130.87, 130.63, 130.46, 130.39, 130.06, 128.55, 127.98, 127.94, 127.90, 107.43, 33.40, 33.10, 31.93, 29.25, 29.18, 24.22, 22.68, 14.16, 13.41.

2.2.9. (Bis(4-(4-methoxyphenyl)phenyl)diphenylsilane (9a)
To a mixture of 7 (1.12 g, 2.26 mmol), potasium carbonate (1.26 g, 9.09 mmol), and 4-methoxyphenylboronic acid 8a (1.01 g, 6.68 mmol) in toluene (25 mL), MeOH (5 mL), and water (5 mL) was added tetrakis(triphenylphosphine)palladium ($Pd(PPh_3)_4$) (0.175 g, 0.152 mmol) at room temperature. The resulting mixture was refluxed with stirring overnight under nitrogen atmosphere. Then the reaction mixture was concentrated under reduced pressure, diluted with water, and extracted with EtOAc. The extract was washed with brine, dried over $MgSO_4$, and concentrated. The residue was purified by silica gel column chromatography (hexane-EtOAc) to give 9a (0.76 g, 46%) as a white powder. Mp=174-176°C.

^{1}H NMR (600 MHz, CDCl3) δ (ppm): δ 7.72– 7.69 (t, J=7.38 Hz, 8H, Ar-H), 7.65– 7.62 (m, 8H, Ar-H), 7.52– 7.49 (t, J=7.17 Hz, 2H, Ar-H), 7.47–7.44 (t, J=7.29 Hz, 4H, Ar-H), 7.04– 7.03 (d, J=6.0 Hz, 4H, Ar-H), 3.90 (s, 6H, Ch3).

^{13}C NMR (151 MHz, $CDCl_3$) δ (ppm): Δ 159.44, 141.90, 136.96, 136.50, 135.78, 135.65, 135.49, 135.30, 134.44, 133.44, 132.28, 129.71, 128.28, 128.01, 127.74, 127.58, 127.36, 127.14, 126.22, 126.02, 114.35, 55.39, 29.80.

2.2.10. Bis(4-(tiophen-2-yl)phenyl)diphenylsilane (9b)
To a mixture of 7 (1.00 g, 2.26 mmol) and 2-(tributylstannyl) thiophene 8b (2.14 g, 6.74 mmol) in dry THF (50 mL) was added tetrakis(triphenylphosphine)palladium $Pd(PPh_3)_4$) (0.521 g, 0.38 mmol) at room temperature. The resulting mixture was refluxed with stirring overnight under nitrogen atmosphere. Then the reaction mixture was concentrated under reduced pressure, diluted with water, and extracted with EtOAc. The extract was washed with brine, dried over $MgSO_4$, and concentrated. The residue was purified by silica gel column chromatography (hexane) to give 9b (0.370 g, 37%) as a silver-blue oil.

^{1}H NMR (600 MHz, $CDCl_3$) δ (ppm): δ 7.68– 7.67 (d, J=6.0 Hz, 4H, Ar-H), 7.44 - 7.42 (t, J=6.0 Hz, 4H, Ar-H), 7.37 (d, J=3.6 Hz, 2H, Ar-H), 7.35 - 7.32 (t, J=9.0 Hz, 2H, Ar-H), 7.26 - 7.25 (d, J=6 Hz, 4H, Ar-H), 7.24– 7.23 (d, J=3.6 Hz, 4H, Ar-H), 7.14 - 7.13 (t, J=4.2 Hz, 2H, Ar-H), 7.07 - 7.06 (t, J=4.2 Hz, 2H, Ar-H).

^{13}C NMR (151 MHz, $CDCl_3$) δ (ppm): δ 144.5, 137.48, 134.48, 128.88, 128.07, 127.04, 127.53, 126.03, 124.87, 124.42, 123.84, 123.15, 29.81.

2.2.11. Bis(4-(acridon-9(10H)-yl)phenyl)diphenylsilane (9c)
To a mixture of 7 (0.95 g, 1.92 mmol) and 9(10H)-acridanone 8c (0.94 g, 4.80 mmol) 0.037 g copper (I) iodide (0.192 mmol) and 0.53 g anhydrous potassium carbonate (3.84 mmol) in DMSO\ THF(20 mL) was added 0.173 g 1,10-phenanthroline (0.960 mmol) at room temperature. The resulting mixture was refluxed with stirring 96 h under nitrogen atmosphere. The reaction was quenched by pouring the reaction mixture into ice-water. The resulting precipitate was filtered off under reduced pressure. The crude product was purified by column chromatography using as eluent a mixture of hexane-ethyl acetate gradient polarity. As a result of the reaction was afforded 0.556 g of bis(4-(acridon-9(10H)-yl)phenyl)diphenylsilane in the form of a pale pink solid in 40% yield. Mp= 234-236°C.

^{1}H NMR (600 MHz, $CDCl_3$) δ (ppm): δ 8.63– 8.62 (d, J=6.0 Hz, 8H, Ar-H), 7.76- 7.73 (t, J=9.0 Hz, 2H, Ar-H), 7.70–7.67 (t, J=9.0 Hz, 2H, Ar-H), 7.55 – 7.52 (t, J=9.0 Hz, 5H, Ar-H), 7.42 -7.24 (d, J=12.0 Hz, 4H, Ar-H), 7.33-7.30 (t, J=9.0 Hz, 5H, Ar-H), 6.80 - 6.78 (d, J=12.0 Hz, 8H, Ar-H).

^{13}C NMR (151 MHz, $CDCl_3$) δ (ppm): δ 178.24, 143.18, 139.02, 135.02, 134.98, 134.94, 134.53, 133.48, 133.31, 132.28, 132.23, 131.93, 131.12, 130.65, 130.59, 130.09, 129.63, 128.89, 128.79, 128.09, 128.01, 127.94, 127.50, 127.35, 121.84, 121.83, 121.80, 121.58, 116.82, 116.53.

2.3 Detailes of theoretical studies
The presented theoretical studies are based on the density functional theory (DFT) methodology [21]. The DFT approach applied here utilizes the Becke's three-parameter functional [22] with the Vosco et al. local correlation part [23] and the Lee et al. [24] nonlocal part, abbreviated as B3LYP. Calculations were performed using the cc-pVDZ basis set [25]. The energies of excited states were calculated within the time-dependent density functional theory (TDDFT) [26]. Then excited stated were included in calculations. The computations were carried out using Gaussian-09 suite of codes [27]. The molecular graphic was produced applying the GaussView software [28].

3. Results and Discussion

Volume - 7 | Issue - 1 | January - 2017 | ISSN - 2249-555X | IF : 3.919 | IC Value : 79.96

3.1. Synthesis

The detail of synthetic route for series of new dithienosilole derivatives are shown in Scheme 1 and 2. The synthetic method used to produce compound 1 was adapted from Huang et al. [11], and offers the facile synthesis of symmetrically 2,6-disubstituted siloles.

The designed macrostructures 4a-g were synthesized by palladium catalyzed Suzuki/Stille coupling reaction of 4-octyl-4-methyl-5,5'-dibromodithienosilole (3) and appropriate dioxaborolane/stannyl derivative of arylenes a-g (Arom), Scheme 1. Solubility of the final compounds (4a-g) were improved significantly by introduction of aliphatic chains [29].

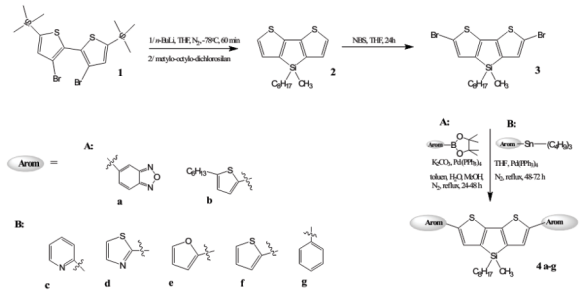

Scheme 1. The synthetic route of the symmetric resulting dithienosilole-based molecules **(4a-g).**

The designed macromolecules 9 a-c were synthesized according to earlier experience [30] by palladium catalyzed Suzuki/Stille condensation and Ullmann reaction of 4,4'-dibromotetraphenylosilane (7) and appropriate dioxaborolane and tributhylstannyl derivative of arylenes a-c (Arom), Scheme 2.

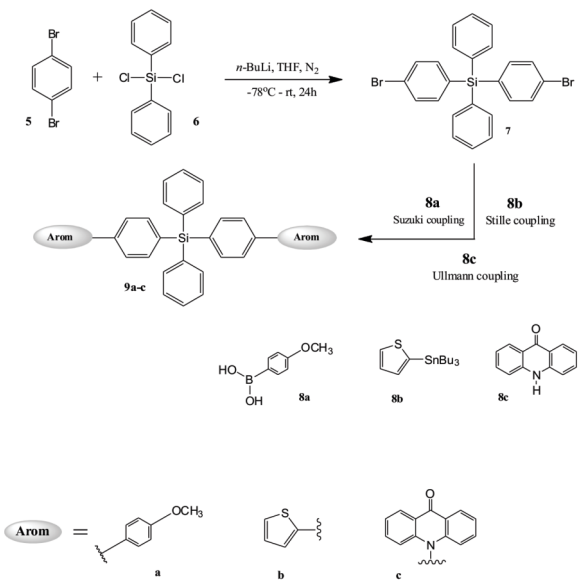

Scheme 2. The pathway for symmetric resulting silole-based heterostructures **(9a-c).**

After each synthetic step, obtained products were purified by the crystallization or the silica column chromatography. Their structures were confirmed and characterized by the 1H NMR, 13C NMR.

3.2. Electrochemical Properties

The electrochemical response of 4b (Fig.1a) consists of a reversible redox pair, centered at 0.26V, followed by two more oxidation signals, the latter of which may be ascribed to over-oxidation, similar to the response of a quaterthiophene. In this case, the inclusion of the terminal alkyl chains both prevents polymerization of the molecule and lowers its ionization potential through an electron-donating inductive effect. Application of strongly negative potentials yields a reduction signal onset, however, this process appears damaging to the compound, as repeated cycling shows a decrease of the observed current in both the reductive and oxidative potential regions.

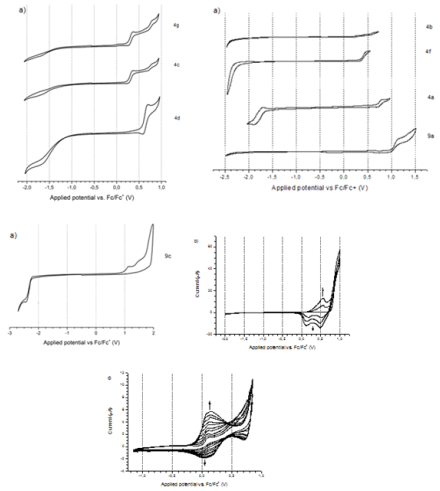

Fig. 1. Electrochemical response of investigated silane derivatives: a) non-dimerizing / non-polymerizing derivatives; b) 9b; c) 4e 1mM solutions of each compound in a 0.1M tetrabutylammonium tetrafluoroborate / dichloromethane supporting electrolyte solution were used. Potential scanning rate r = 0.1V/s.

The above compound, 4b is prepared from another of the investigated systems 4f, by grafting two terminal alkyl chain substituents onto the conjugated system. Concurrent with the lack of electron-donating substituents, only one oxidation step is observed for 4f, featuring at best partial reversibility and located at 0.40V, in comparison to the first oxidation signal of 4b being observed at 0.26V. Although polymerization is not observed upon repeated cycling of a 1mM solution of 4f, increasing its concentration up to near-saturation, at 10mM shows changes in the electrochemical response upon potential cycling (Fig. S01, supplement materials). Even so, no signals at less positive potentials evolve, indicating that the occurring process is not dimerization, but possibly electro-precipitation and solubilization on the electrode surface.

The cyclic voltammograms of 4c and 4g (Fig. 1a) both consist of a semi-reversible redox pair at 0.31V and an oxidation peak at higher potentials, of 0.83 and 0.81V respectively. The low-potential redox pair is attributed to the oxidation of the dithienosililol moiety and its subsequent reduction to the electroneutral moiety. The reduction signal is less pronounced than the oxidation peak, indicating partial irreversibility, possibly implying that the high-potential (0.8V) oxidation peak is over-oxidative in nature. Conversely, the lack of an influence of the substituent on the potential of the redox pair (0.31V) is evidence for lack of conjugation between the central moiety and the terminal phenyl or pirydyl substituents. The negative potential end of both CVs lacks any distinctive features apart from an inflection point at approx. -1.7V, due to the fact that the electron-donating nature of the dithienosililol moiety.

When the dithienosililol is substituted by the weakly electron-withdrawing thiazole moieties, however, a significant shift in the potential of the dithienosililol redox pair occurs, as it is observed at 0.64V for 4d. The attributed over-oxidative signal is absent at high-potentials, possibly due to extended conjugation and, consequently, improved capability of accommodating charges. This implied stability is further indicated by EPR investigation (Fig. 6e), as 4d is the only one of the three studied compounds, whose radical cation can be observed.

The voltammetric behaviour of 4a in dichloromethane features two redox pairs, centered respectively at -1.79V and at 0.75V (Fig. 1a). In

Volume - 7 | Issue - 1 | January - 2017 | ISSN - 2249-555X | IF : 3.919 | IC Value : 79.96

the case of the positive potential redox pair, the cathodic peak is significantly less pronounced, indicating the occurrence of a competing chemical reaction. Upon repeated potential sweeping, no new signals are generated, indicating that this reaction is electro-deactivating in its nature. Considering the similarity of the electron-donating bisthienosilol moiety to bithiophene, we can hypothesize that the mechanism of this process is analogous to the over-oxidative degradation of bithiophene.

The CV of 9a features a sharp oxidation peak at approximately 1.15V, corresponding to the oxidation of the aromatic ring system (Fig. 1a). The relatively low potential, at which the abstraction of the first electron from the system takes place, implies that at least partial conjugation exists within the 9a molecule. This oxidation signal is closely followed by and partially overlaps another signal, which may be over-oxidative in nature. This claim is supported by the fact, that upon reversing the potential scan polarity, a reduction signal is observed at 0.80V. However, its magnitude is far lesser than that of the oxidation signals, indicating that the population of the oxidized species was diminished. Repeated potential cycling does not bring about the evolution of signals at less positive potentials, ruling out the formation of a product featuring improved conjugation.

The cyclic voltammogram (CV) of 9c in dichloromethane (Fig. 1a) features a redox pair centred at -2.32V, related to the reduction of the phenoxazine moiety. The lack of pronounced peaks at the standard potential scanning rate indicates that the electron transfer process occurs relatively rapidly. The pre-peak at approx. 1.14V can be attributed to specific adsorption, whereas the presence of an irreversible oxidation peak at 1.9V indicates that the oxidised species undergo a consecutive chemical reaction. Subsequent potential sweeps of the experimental solution reveal that this process does not involve elongation of the conjugated bond system, as no new signals at less positive potentials are produced. Using the onsets of the reduction peak (-2.25V) and the oxidation signal (1.63V), the electron affinity and ionisation potentials are determined, indicating a frontier molecular orbital energy gap of 3.88eV (Table 1), slightly deviating from the value of 4.29eV, obtained from the slope of the ground-state optical absorption signal of the compound (Fig. S02a). In this case, the slope of the higher energy absorption signal was used, as the structure of the absorption signal centred at 370nm (3.35eV) arises from oxidised phenoxazine moieties, whose presence may be a result of the procedure used for the synthesis of 9c.

The electrochemical response of a 9b solution features a sharp oxidation signal, with an onset at 0.77V, coupled with rapid deposition of a solid-state film on the working electrode (Fig. 1b). When the scan polarity is reversed, two reduction signals are observed at 0.51V and 0.19V. Further potential sweeps show fast evolution of these signals, along with a single oxidation peak at 0.57V, indicating that polymerization indeed takes place. The lack of a pronounced oxidation peak, corresponding to the 0.19V reduction signal, indicates that the first oxidation stage proceeds much more rapidly than the second. This can be explained by the fact that the first oxidation stage corresponds to the oxidation of the 2,5'-bithienylene moiety present in the expected polymer structure, whereas the second stage involves a change in the geometry of the molecule, extending conjugation onto the phenylene rings surrounding the 2,5'-bithienylene moiety and abstraction of a second electron from this system.

The polymerization of 9b has been followed by fast, time-resolved UV-Vis-spectroelectrochemistry (Fig. 2), revealing the layer-by-layer deposition of a solid-state film on the ITO/quartz electrode, with an absorption maximum at 435nm in its ground state and an oxidized state absorption extending into the NIR region. When the obtained deposit is investigated by scanning the applied potential in the range used for its preparation, no noticeable loss of absorbance or electrochemical response is observed over twenty potential cycles, evidencing its good stability. The response time of the deposit is relatively low, however, further optimization of the layer thickness for the purpose of electrochromic device applications is definitely possible.

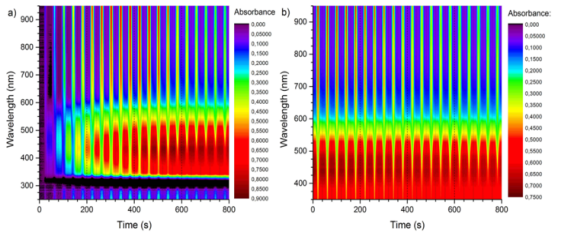

Fig. 2. Fast, time-resolved UV-Vis spectroelectrochemistry of a) 1mM solution of 9b in supporting electrolyte; b) **poly(9b)** solid layer on an ITO/quartz electrode in supporting electrolyte. Contour plots show UV-Vis absorbance spectra (corrected for monomer and supporting electrolyte absorption), registered continuously during twenty consecutive potential scans. Scan speed 0.1V/s, Potential range applied to the working ITO/quartz electrode: -0.5V to +1.5V vs. Ag/Ag+.

The CV of 4e features an oxidation peak at 0.10V and an irreversible oxidation onset at 0.96V (Fig. 1c). Cycling the potential in the range including this second oxidation signal or beyond it results in the evolution of a redox system, incorporating the oxidation peak at 0.10V. Consequently, the presence of the peak at 0.10V in the monomer solution is ascribed to traces of the polymer, indicating the high reactivity of 4e. Even though repeated potential cycling brings about an increase in peak currents, no solid-state deposit is found at the electrode, unless the monomer concentration is raised up to 10mM (Fig. 3). When a poly(4e) -coated electrode is subjected to potential cycling in a supporting electrolyte solution, the electro-chemical response of the polymer film diminishes rapidly, indicating that the deposit is not stable even under polymerization conditions.

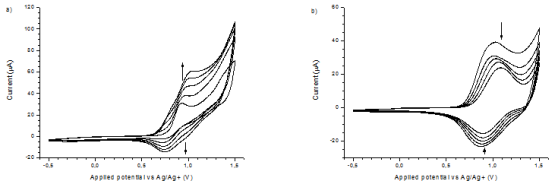

Fig. 3. a) Electrochemical deposition of a thin solid layer from a 10mM solution of **4e**; b) Electrochemical response of the deposited layer.

The electropolymerization process of 4e has also been studied through fast, time-resolved UV-Vis spectroelectrochemistry (Fig. 4), showing a slow evolution of an absorption signal at 480nm, corresponding to the ground state of the oligomer, as well as wider signals at higher wavelengths, corresponding to p-doped states of the oligomer.

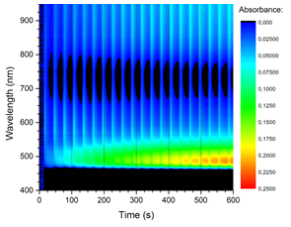

Fig. 4. Fast, time-resolved UV-Vis spectroelectrochemistry of a 1mM solution of **4e** in supporting electrolyte. Contour plot shows UV-Vis absorbance spectra (corrected for monomer and supporting electrolyte absorption), registered continuously during twenty consecutive potential scans. Scan speed 0.1V/s, potential range applied to the working ITO/quartz electrode: -0.5V to 1.5V vs. Ag/Ag+.

Volume - 7 | Issue - 1 | January - 2017 | ISSN - 2249-555X | IF : 3.919 | IC Value : 79.96

The discrepancies between the energy gaps determined electrochemically and spectrally (Table 1) are relatively low, with two compounds being excluded from the comparison due to the fact that their reduction potentials are sufficiently negative that polymerization at the counter electrode becomes an issue in the measurement.

Table 1. Electrochemical and theoretical properties of investigated compounds.

Compound	Reduction potential (V)a	Electron affinity (eV)b	Oxidation potential (V)a	Ionisation potential (eV)b	Theor. vertical ionisation energy (eV)	Theor. adiabatic ionisation energy (eV)	Electrochemical frontier orbital energy gap (eV)c	Optical frontier orbital energy gap (eV)c	HOMO/LUMO gap (eV)
4a	-1.66	3.44	0.70	5.80	6.49	6.38	2.36	2.43	2.43
4b	-2.33	2.77	0.19	5.29	5.62	5.58	2.52	2.53	2.47
4c	-1.30	3.80	0.25	5.35	6.25	6.25	1.55	-	3.11
4d	-1.24	3.86	0.57	5.67	6.46	6.40	1.80	-	2.95
4e	-d	-	0.96	6.06	5.93	5.93	-	2.56	2.97
4f	-2.28	2.82	0.36	5.46	5.97	5.74	2.64	2.58	3.06
4g	-1.36	3.74	0.25	5.35	6.30	6.12	1.61	-	3.23
9a	-2.32	2.78	1.01	6.11	6.61	6.60	3.33	3.87	4.73
9b	-d	-	0.77	5.87	6.83	6.78	-	3.61	4.47
9c	-2.25	2.85	1.63	6.73	6.33	6.33	3.88	4.29	3.81

a. onset potentials vs. Ferrocene / Ferrocinium standard redox couple (Fig. 1)
b. calculated using equations: Electron affinity = $|e|\cdot(5.1 + ERED)$; Ionisation potential = $|e|\cdot(5.1 + EOX)$
c. calculated from UV-Vis-NIR spectra (Fig. 5)
d. reduction potential impossible to determine due to the occurrence of electrodeposition at the counter electrode

The UV-Vis-NIR spectra (Fig. 5) of the investigated compounds, apart from 9a and 9b, each consist of two absorption signals – one in the deep UV and one located on the threshold between the UV and Vis ranges, indicating that while conjugation extends over most of their structure, explaining the low-energy absorption signal, it does not span across the entire molecule, giving rise to absorption from what we believe to be individual aromatic rings.

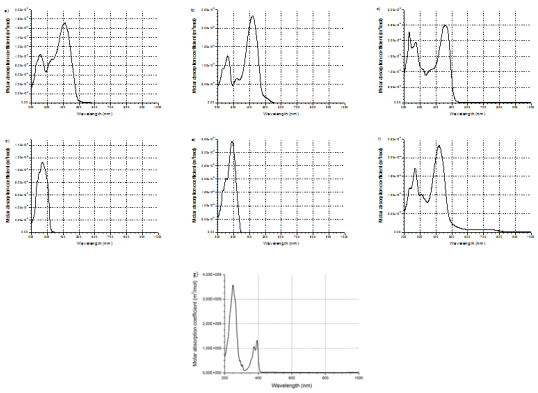

Fig. 5. UV-Vis-NIR spectra of investigated compounds a) **4b;** b) **4f;** c) **4a ;** d) **9a;** e) **9b;** f) **4e** g) **9c**

The absorption spectrum of 9a features one composite absorption signal in the UV range, composed of three overlapping signals. This signal originates from the individual and non-conjugated phenyl and phenylene rings within the molecule and its constituents can be ascribed, in order of decreasing maximum absorption wavelength, to the terminal p-metoxyphenylene rings, the middle phenylene rings and the phenyl substituents attached to the silicon atom.

In the case of 9b, the spectrum consists of a single UV range absorption signal, indicating little to no conjugation between the thienyl and phenylene groups, as expected theoretically. Interestingly, this appears to change upon application of oxidizing potentials, as discussed earlier.

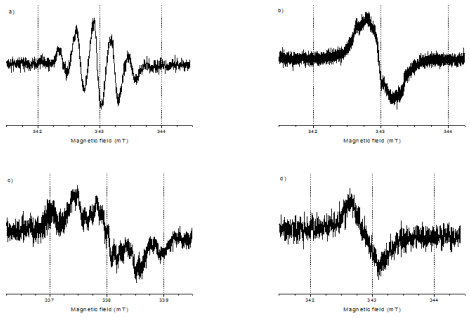

Fig. 6. Electron paramagnetic resonance spectra of species electrogenerated from the investigated compounds a) **4b** radical cation; b) **4f** radical cation; c) **4a** radical anion; d) **9a** radical cation; e) **4d** radical cation

The EPR spectrum of a 4b radical cation is a complex multiplet, with nine lines being registered (see Fig. S02, supplement materials) for the absorption spectrum) and originating from a single type of species (Fig. 6a). The chemical structure of 4b lacks any nuclei possessing a spin of 1 or more. Consequently, the multiplet nature of the signal is ascribed to interactions of the radical cation with no less than eight neighbouring protons. Identification of the particular protons interacting with the radical cation is beyond the scope of this work. Conversely, the EPR spectrum of a 4f radical cation consists of a singlet. Comparison with 4b indicates that the protons of the two terminal alkyl chain substituents, found in 4b, are among those interacting with its radical cation and giving rise to the observed hyperfine structure.

Investigation of the radical anions, generated from 4a (Fig. 6c) reveals a rich hyperfine structure. The influence of two nitrogen atoms can be observed, indicating that the radical anion is localized on the benzoxadiazole moiety. Interactions with the neighbouring hydrogen atoms of the benzoxadiazole moiety are observed and expected.

The EPR spectrum of a 9a radical cation consists of a broad singlet, likely arising from a radical cation localized mostly on the methoxy-substituted phenylene ring (Fig. 6d). Although interactions with the protons attached to the phenylene ring would be expected, their splitting constants may be insufficiently high to manifest a hyperfine structure, in light of the significant line width of this species.

3.3. Optical Spectroscopic Properties

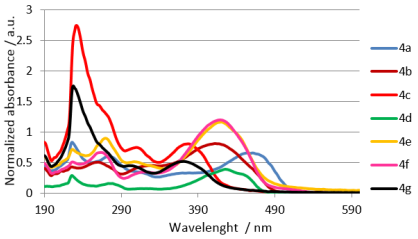

Fig. 7. Normalized absorption spectra of the dithienosilole derivatives **(4a-g)** in dichloromethane solution (10^{-6} mol/dm^3)

Normalized UV-Vis absorption spectra and emission spectra of the synthesized copolymers in CH_2Cl_2 solution are shown on Figure 7 and

Volume - 7 | Issue - 1 | January - 2017 | ISSN - 2249-555X | IF : 3.919 | IC Value : 79.96

Figure 8, and the optical properties of the dithienosilole derivatives are summarized in Table 2. Compounds 4c exhibited three major absorption bands. The first one is located in the high energy 240-250 nm region, corresponding to the spin-allowed, π-π* adsorption of peripheral pyridine groups. The second covers the lower energy 295-330 nm region, corresponding to the π-π* absorption induced by the large conjugative pyridines (a pronounced vibronic peak). Finally, the weakest one- at the lowest energy 360-410 nm region- were attributed to the forbidden n-π* absorption. Similar situation was observed in the cause of compounds 4g. The C-Si bond is significantly longer than the C– C bond, which leads to the red shift and the vibronic peak of absorbance [19].

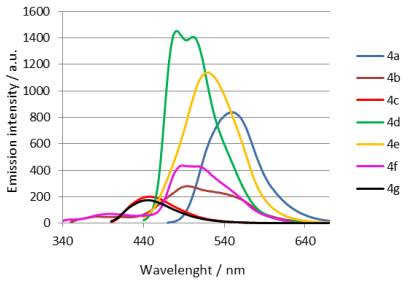

Fig. 8. Emission spectra of the **4a-g** in dichloromethane solution (10^{-6} mol/dm^3)

Furthermore, compounds 4a-g are all luminescent. 4c and 4g emit a violet-blue color in solution and the rest of compounds 4a,b,d-f emit the light in region from blue to red. Moreover, the large Stokes shifts above 4200 cm^{-1} [31] of the 4e and 4g (Table 2) suggest applications of this compounds as effective fluorescent dyes. Further the emit the red light in the solid state when irradiated by UV light (Fig. 9), what makes compound 4a a potential emitter in organic electroluminescence devices (OLED) and solid-state dye laser.

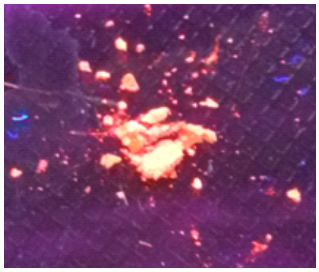

Fig. 9. Emission red light in solid state of **4a** by irradiation UV light

Table 2. Electronic transitions in absorption spectra (nm) of dithienosilole derivatives

Macrostructure	λ_{Abs} [nm]	λ_{Abs} Theoretical [nm]	λ_{Em} [nm]	Stokes shift $\Delta\nu^a$ [cm^{-1}]
4a	461	553 (HOMO→LUMO)	548	3444
4b	412	478 (HOMO→LUMO)	496	4110
4c	378	434 (HOMO→LUMO)	447	4084
4d	426	453 (HOMO→LUMO)	481, 501	2684, 3514
4e	420	451 (HOMO→LUMO)	521	4616
4f	420	443 (HOMO→LUMO)	489, 509	3360, 4163
4g	371	423 (HOMO→LUMO)	445	4482
9a	278	288 (HOMO→LUMO)	339	6473
9b	292	272 (HOMO→LUMO)	348	5511
9c	375, 393	365 (HOMO→LUMO+1)	408, 426	2157, 1971

[a] $\Delta\nu=1/\lambda_{Abs}-1/\lambda_{Em}$ [cm^{-1}]

Figure 10 and 11 present normalized absorbance and photoluminescence spectra of the silicon-bridged compounds. The absorbance spectrum of 9a and 9b reveals a broad featureless absorption peak at 278 nm for 9a and 292 nm for 9b. Notably, the absorbance spectrum of 9c displays a markedly redshifted absorption (375 nm and 393 nm) relative to 9a and 9b. These features indicate that the silole ring enhances the conjugation and interactions of the nitrogen atoms from acridone moiety. The emission spectra reveal very similar behavior. For compound 9a and 9b the photoluminescence emission is in the violet and blue region with large Stokes shifts. Compound 9c emits the light in blue and green region with maximum centered at 408 nm and 426 nm.

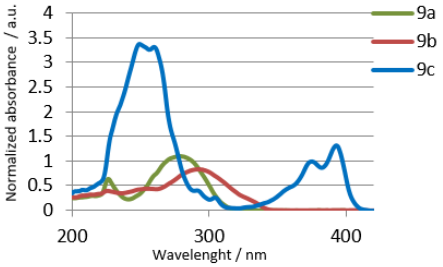

Fig. 10. Normalized absorption spectra of the tetraphenylsilane derivatives **(9a-c)** in dichloromethane solution (10^{-5} mol/dm^3)

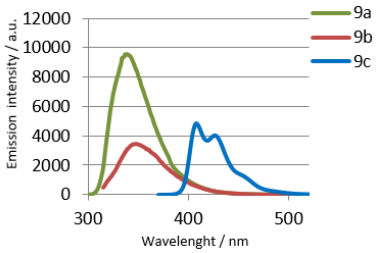

Fig. 11. Emission spectra of the **9a-c** in dichloromethane solution (10^{-5} mol/dm^3)

3.4. Theoretical Studies

Analysis of the geometry of orbitals HOMO/LUMO optimized compounds demonstrates their total distribution on the heteroaromatic moieties in the molecule. In addition, the planarity of designed dithienosilole derivatives, supports their conductive properties (Fig. 12). Comparing the derivatives 4b and 4f, it is not observed the effect of aliphatic chain of 5-hexylthiophene (4b) on the electronic structure of the compounds. Moreover, the compound 4b has about 0.59 eV smaller band gap value compared to compound 4f (Table 1, Fig. 13). The value of the energy gap obtained by theoretical calculations, correlate very well with the results of Eg value determined using UV-Vis spectra. The lowest band gap (2.43 eV) has a compound 4a, and the greatest Eg (3.23 eV) possess a derivative containing a phenyl moiety (4g). These values are different from the results obtained electrochemically, wherein the compound 4c has the smallest band gap (1.55 eV). These differences are observed, although, in both electrochemical and optical Eg value, the transition takes place between the HOMO and LUMO orbitals.

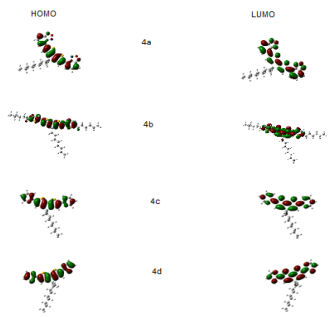

Volume - 7 | Issue - 1 | January - 2017 | ISSN - 2249-555X | IF : 3.919 | IC Value : 79.96

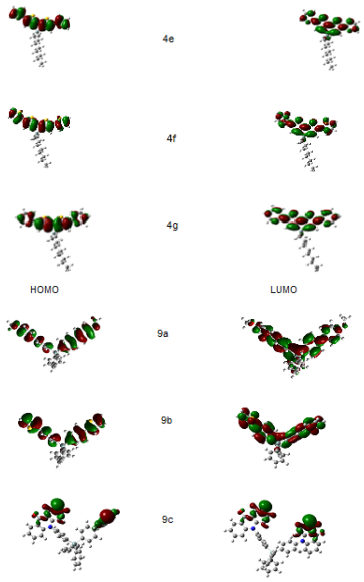

Fig. 12. HOMO and LUMO contour plots for studied compounds

The high located LUMO energy level, reduced the electron injection barrier and thus the ability of the charge injection is greater (Fig. 13). In addition, the relatively low value of ionization potentials of the dithienosilole derivatives, suggests that these compounds possess a good conductive properties. For 9c results showed the interruption of conjugation between the acridone groups by tetrahedral silica core, which suggests that the 9c is a full charge transfer compound. Moreover, the 9c has the smallest value of the band gap of the remaining tetraphenylsilane derivatives. For 9a and 9b compounds the HOMO/LUMO orbitals are distributed over the entire structure. Introduction of a methoxyphenyl groups to the tetraphenylsilane core (9a) causes considerably increases the LUMO energy, so that the band gap value is increased by 0.52 eV (in comparison to 9c).

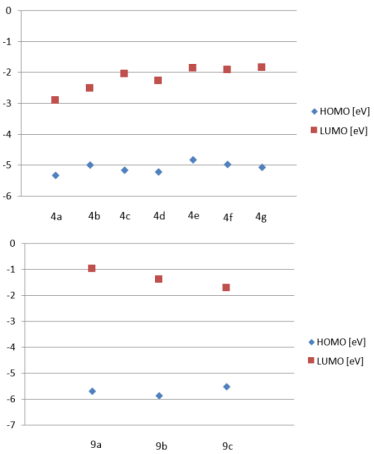

Fig. 13. The EHOMO, ELUMO levels for **4a-g** and **9a-c** compounds

SUPPLEMENT MATERIALS

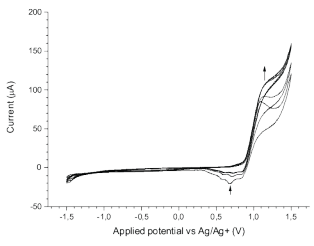

Fig. S01. Electrochemical response of a 10mM solution of **4f** upon repeated potential cycling.

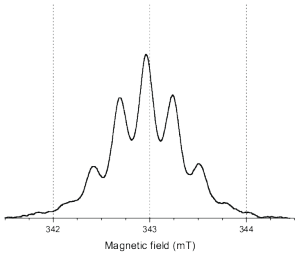

Fig. S02. Electron paramagnetic resonance absorption spectrum of the **4b** radical cation. The spectrum was obtained by a single integration of the experimental first derivative spectrum, presented in Fig. 6a.

4. Conclusions and Remarks

Synthesized dithienosilole-based molecules with push-pull structure, demonstrate unusual advantages in the field of modern electronic materials. The results presented here report the synthesis and the physicochemical investigation of macromolecules based on dithienosilole. These structures were synthesized by the Suzuki/Stille condensation with fine yield. All obtained compounds are electronically and optically active. These macrostuctures in solution indicate clear light absorption covering the region from 230 to 500 nm. Moreover, the dithienosiloles (4a-g) exhibit light emission in nearly the entire visible region. The cyclic voltammetry was adapted to find the electrochemical behavior of the derivatives. The onset of the oxidation signal was observed at fairly low potentials. The optical band gap, found between 2.53 eV (4a) and 3.87 eV (9a), creates the compounds potentially utilized as an hosting medium for emitters and hole/electron blocking film in the OLEDs display. The lowest electrochemical and optical band gap describes symmetric unit including dithienosilane moiety (4a), the largest - structure with p-phenylenomethoxy group. Electrochemical features of studied macrostructures make this material of interest for electrochromic applications. Furthermore, EPR spectra supply little information about the architecture of the electro-generated radical cations. The effects of electrochemical research certify that tetraphenylsilane system sufficiently interrupts transmission between each moiety and keeps to separated schedules of HOMO and LUMO levels, further depicting that the bipolar design policy adapting an insulator tetraphenylsilane as the linkage can retain from blue to red emission and facilitate device acting as an effect of a lower charge injection barrier. Consequently, the combination of silane-based, electron-transport mediums presents the best results in i.e. OLED devices.

Acknowledgment

To the financial support from a Grant of a statutory activity subsidy from Polish Ministry of Science and Technology of Higher Education for the Faculty of Chemistry of Wroclaw University of Science and Technology. The Authors would like also to thank Wroclaw Centre of Computing and Networking for generous allotment of computer time.

References

1. K. Tamao, M. Uchida, T. Izumizawa, K. Furukawa, S. Yamaguchi, J. Am. Chem. Soc. 118 (1996) 11974-11975.
2. K. L. Chan, M. J. McKiernan, C. R. Towns, A. B. Holmes, J. Am. Chem. Soc. 127 (2005) 7662-7663.
3. J. Chen, C. C. W. Law, J. W. Y. Lam, Y. Dong, S. M. F. Lo, I. D. Williams, D. Zhu, B. Z. Tang, Chem. Mater. 15 (2003) 1535-1546.
4. H. Park, Y. Rao, M. Varlan, J. Kim, S.-B. Ko, S. Wang, Y. Kang, Tetrahedron, 68 (2012) 9278-9283.
5. J. Ohshita, Y. Tominaga, D. Tanaka, Y. Ooyama, T. Mizumo, N. Kobayashi, H. Higashimura, Dalton Trans. 42 (2013) 3646-3652.
6. J. C. Sanchez, S. A. Urbas, S. J. Toal, A. G. DiPasquale, A. L. Rheingold, W. C. Trogler, Macromol. 41 (2008) 1237-1245.
7. A. Laguna (Ed.). Modern Supramolecular Gold Chemistry. Wiley, 2009.
8. J. Chen, Y. Cao, Macromol. Rapid Commun. 28 (2007) 1714-1742.

Volume - 7 | Issue - 1 | January - 2017 | ISSN - 2249-555X | IF : 3.919 | IC Value : 79.96

9. V. W. –W. Yam, E. C. -C. Cheng, Chem. Soc. Rev. 37 (2008) 1806–1813.
10. R. Grisorio, G. P. Suranna, P. Mastrorilli, G.Allegretta,A. Loiudice, A.Rizzo, G. Gigli, K. Manoli, M. Magliulo, L. Torsi, J. Polym. Sci., Part A: Polym. Chem. 51 (2013) 4860–4872.
11. J. H. Huang, C.-M. Teng, Y. S. Hsiao, F. W. Yen, P. Chen, F. C. Chang, C. W. Chu, J. Phys. Chem. C, 115 (2011) 2398–2405.
12. H. Medlej, H. Awada, M. Abbas, G. Wantz, A. Bousquet, E. Grelet, K. Hariri, T. Hamieh, R. C. Hiorns, C. Dagron-Lartigau, Euro. Polym. J. 49 (2013) 4176–4188.
13. J. Huang, Y. Ie, M. Karakawa, M. Saito, I. Osaka, Y. Aso, Chem. Mater. 26 (2014) 6971–6978.
14. J. A. Love, I. Nagao, Y. Huang, M. Kuik, V. Gupta, C. J. Takacs, J. E. Coughlin, L. Qi, T. S. van der Poll, E. J. Kramer, A. J. Heeger, T.-Q. Nguyen, G. C. Bazan, J. Am. Chem. Soc. 136 (2014) 3597-3606.
15. H. Huang, J. Youn, R. P. Ortiz, Y. Zheng, A. Facchetti, T. Marks, Chem. Mater. 23 (2011) 2185–2200.
16. W. Kang, M. Jung, W. Cha, S. Jang, Y. Yoon, H. Kim, H. J. Son, D.-K. Lee, B. S. Kim, J. H. Cho, ACS Appl. Mater. Interfaces, 6 (2014) 6589–6597.
17. X. Zhan, A. Haldi, C. Risko, C. K. Chan, W. Zhao, T. V. Timofeeva, A. Korlyukov, M. Y. Antipin, S. Montgomery, E. Thompson, Z. An, B. Domercq, S. Barlow, A. Kahn, B. Kippelen, J.-L. Bredas, S. R. Marder, J. Mater. Chem. 18 (2008) 3157-3166.
18. K. Tamao, M. Uchida, T. Izumizawa, K. Furukawa, S. Yamaguchi, J. Am. Chem. Soc. 118 (1996) 11974-11975.
19. H. Y Chen, J. Hou, A. E. Hayden, H. Yang, K. N. Houk, Y. Yang, Adv. Mater. 22 (2010) 371-375.
20. H. Jung, H. Hwang, K.-M. Park, J. Kim, D.-H. Kim, Y. Kang, Organometallics, 29 (2010) 2715–2723.
21. R.G. Parr, W. Yang, Density Functional Theory of Atoms and Molecules, Oxford University Press, 1994.
22. A.D. Becke, J. Chem. Phys. 98 (1993) 5648-5652.
23. S.H. Vosco, L. Wilk, M. Nusair, Can. J. Phys. 58 (1980) 1200-1211.
24. C. Lee, W. Yang, R.G. Parr, Phys. Rev. B, 37 (1988) 785-789.
25. T.H. Dunning, J. Chem. Phys. 90 (1989) 1007-1023.
26. M. A. L. Marques, C.A. Ullrich, F. Nogueira, A. Rubio, K. Burke, E.K.U. Gross (Eds.), Time-Dependent Density Functional Theory, Springer-Verlag, 2006.
27. Gaussian 09, Revision E.01, M. J. Frisch, G. W. Trucks, H. B. Schlegel, G. E. Scuseria, M. A. Robb, J. R. Cheeseman, G. Scalmani, V. Barone, B. Mennucci, G. A. Petersson, H. Nakatsuji, M. Caricato, X. Li, H. P. Hratchian, A. F. Izmaylov, J. Bloino, G. Zheng, J. L. Sonnenberg, M. Hada, M. Ehara, K. Toyota, R. Fukuda, J. Hasegawa, M. Ishida, T. Nakajima, Y. Honda, O. Kitao, H. Nakai, T. Vreven, J. A. Montgomery, Jr., J. E. Peralta, F. Ogliaro, M. Bearpark, J. J. Heyd, E. Brothers, K. N. Kudin, V. N. Staroverov, R. Kobayashi, J. Normand, K. Raghavachari, A. Rendell, J. C. Burant, S. S. Iyengar, J. Tomasi, M. Cossi, N. Rega, J. M. Millam, M. Klene, J. E. Knox, J. B. Cross, V. Bakken, C. Adamo, J. Jaramillo, R. Gomperts, R. E. Stratmann, O. Yazyev, A. J. Austin, R. Cammi, C. Pomelli, J. W. Ochterski, R. L. Martin, K. Morokuma, V. G. Zakrzewski, G. A. Voth, P. Salvador, J. J. Dannenberg, S. Dapprich, A. D. Daniels, Ö. Farkas, J. B. Foresman, J. V. Ortiz, J. Cioslowski, and D. J. Fox, Gaussian, Inc., Wallingford CT, 2009.
28. GaussView 3.0, Gaussian, Inc., Carnegie Office Park – Building 6, Pittsburgh, PA, USA.
29. M. Wang, C. Li, A. Lv, Z. Wang, Z. Bo, F. Zhang, Polym. 53 (2012) 324-332.
30. D. Zając, J. Sołoducho, T. Jarosz, M. Łapkowski, S. Roszak, Electrochim. Acta, 173 (2015) 105-116.
31. F. Vollmer, W. Rettig, E. Birckner, J. Fluoresc. 4 (1994) 65–69.